LETTERS
https://doi.org/10.1038/s41567-022-01535-w

nature physics

Strong coupling of alkali-metal spins to noble-gas spins with an hour-long coherence time

R. Shaham [1,2,4] ✉, O. Katz [1,2,3,4] and O. Firstenberg [1]

Nuclear spins of noble gases can maintain coherence for hours at ambient conditions because they are isolated by complete electron shells[1]. This isolation, however, impedes the ability to manipulate and control them by optical means or by coupling to other spin gases[2–4]. Here we achieve strong coherent coupling between noble-gas spins and the optically accessible spins of an alkali-metal vapour. The coupling emerges from the coherent accumulation of stochastic spin-exchange collisions. We obtain a coupling strength ten times higher than the decay rate, observe the coherent and periodic exchange of spin excitations between the two gases and demonstrate active control over the coupling by an external magnetic field. This approach could be developed into a fast and efficient interface for noble-gas spins, enabling applications in quantum sensing and information[5,6].

Noble-gas isotopes with non-zero nuclear spin, such as helium-3, feature day-long spin lifetimes and hours-long coherence times[1,7]. They are prominent in various fields, from precision sensing[8–11] and medical imaging[12] to searches for new physics[13–17], and they hold promise for future quantum information applications such as optical quantum memories and the generation of long-lived entanglement[5,18–21]. The latter rely on the feasibility of preparing the collective spin state of the gas and controlling its quantum excitations[22].

Polarized ensembles of alkali-metal spins or noble-gas spins can carry such collective excitations, corresponding classically to a tilt of the collective spin about the polarization axis[23]. These can be modelled as quantum excitations of a harmonic oscillator. Remarkably, the quantum description persists even for gaseous ensembles undergoing rapid diffusion[24,25] and for overlapping ensembles that interact via atomic collisions[22,26–28]. The collective state of alkali-metal spins can be addressed and coherently controlled by optical means[29–31]. The same, however, cannot be done for the nuclear spins of noble gases, which lack any optical transition from the ground levels. Instead, one can access the noble-gas spins by collisions with another spin gas, either excited (metastable) helium-3 or alkali-metal vapour, both of which possess optically accessible spin[1,32,33].

Alkali-metal atoms exchange spin with noble-gas atoms via a weak electron–nuclear coupling (Fermi contact) during collisions[34]. They are normally used for hyperpolarizing the noble gas and for probing its spin dynamics. The probing relies on the coherent component of the spin-exchange interaction, which is usually weak and manifests as a shift in the precession frequencies of the alkali-metal spins. The coherent component is employed for the readout of noble-gas-based sensors and for inherent suppression of sensitivity to magnetic fields[2–4,9].

In ref. [3], Kornack and Romalis employed the coherent component of the spin-exchange interaction to study the hybridization of the collective spins of alkali-metal and noble-gas ensembles in the critical damping regime. By varying the axial magnetic field, they observed shortening of the noble-gas spin coherence time and shifting of the noble-gas magnetic resonance due to the alkali-metal spin dressing. With a coupling rate lower than the alkali-metal decay rate, they observed the onset of avoided crossing in the magnetic spectrum but did not record reversible dynamics or revivals of the spin. In ref. [35], we reported on using alkali-metal spins as off-resonant mediators to couple light to noble-gas spins bidirectionally. These and all other studies so far have been limited to the detuned or critical coupling regimes.

Increasing the coupling rate between the spin gases is beneficial to various applications. When the coupling exceeds the alkali-metal decay rate, the dynamics of the spin gases become strongly coupled, enabling rapid and coherent control of the noble-gas spins. Operation in this strong-coupling regime opens new practical avenues, especially for in-and-out mapping of quantum states, for enhancing the indirect interaction of noble-gas spins with photons and for improving the performance of sensing applications[6,18,22]. Yet, strongly coupled dynamics and, in particular, the reversible exchange between the spin gases have never been demonstrated.

Here we report on strong coherent coupling between the collective spin states of noble-gas and alkali-metal ensembles. We enter the strong-coupling regime by reaching high polarizations and densities of the interacting species while minimizing spin relaxation. We directly probe the dynamics of both spin ensembles and demonstrate the coherent and reversible exchange of excitations between them. These results demonstrate that stochastic spin-exchange collisions which are individually weak but together frequent enough can accumulate to form an efficient coherent interface between two spin gases. We discuss prospects for strongly coupled gases and their potential utility in classical and quantum applications.

To characterize the exchange, we consider the bosonic, collective, spin excitations of the alkali-metal and noble-gas spins, represented by the annihilation operators $\hat{a}$ and $\hat{b}$, respectively. The coupling between these excitations relies on the collective enhancement of the exchange interaction due to the accumulation of numerous collisions among the two spin ensembles. The collective, bidirectional, coupling rate $J=(\tilde{\zeta}/2)\sqrt{n_a p_a n_b p_b}$ thus depends on the square root of the atomic densities n_a and n_b and the degrees of polarization $0 \leq p_a \leq 1$ and $0 \leq p_b \leq 1$ (ref. [22]). The microscopic coupling strength $\tilde{\zeta}(p_a)$, incorporating the collisional cross-section, has a weak dependence on the alkali-metal spin polarization due to the hyperfine structure of the alkali-metal atoms (Methods). A simple form of two coupled modes can be used to describe the exchange dynamics

[1]Department of Physics of Complex Systems, Weizmann Institute of Science, Rehovot, Israel. [2]Rafael Ltd, Haifa, Israel. [3]Present address: Department of Electrical and Computer Engineering, Duke University, Durham, NC, USA. [4]These authors contributed equally: R. Shaham, O. Katz. ✉e-mail: roy.shaham@weizmann.ac.il

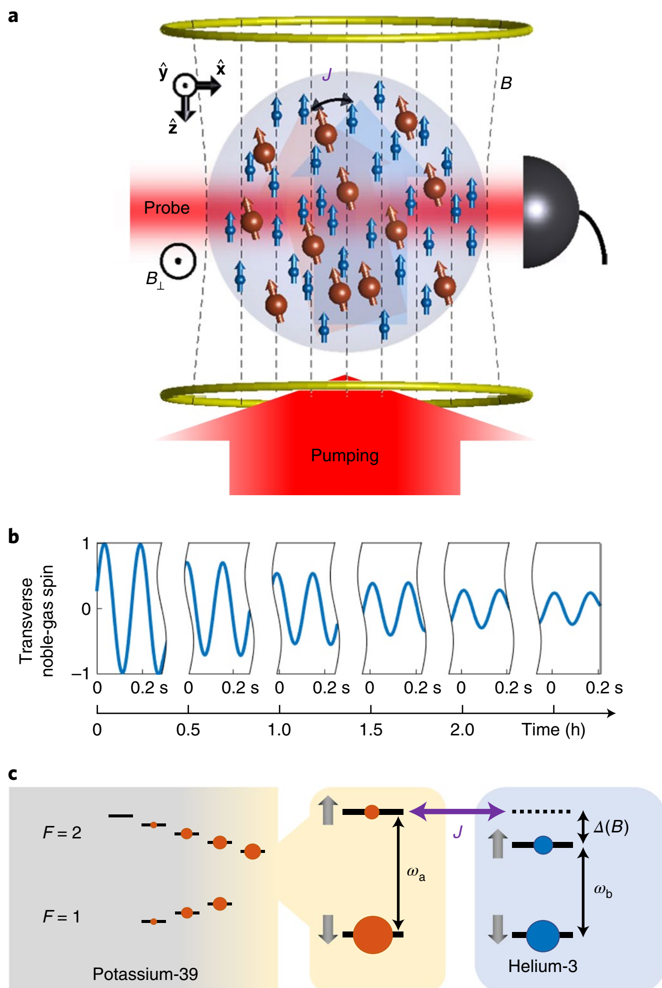

Fig. 1 | Experimental scheme and coherence time measurements. **a**, A glass cell containing optically pumped potassium vapour (alkali-metal spins, red) and helium-3 (noble-gas spins, blue). The polarized ensembles couple via stochastic atomic collisions that accumulate to a collective spin-exchange interaction at a rate J. An applied magnetic field $B\hat{\mathbf{z}}$ controls the precession frequency difference $\Delta=\omega_a-\omega_b$ between the two ensembles. A transverse excitation of the spins is initialized by a short transverse magnetic field pulse $B_\perp\hat{\mathbf{y}}$ and then monitored by Faraday rotation of an optical probe. **b**, Precession of the helium-3 spins, measured at low spin polarizations and normalized to the initial value, featuring a coherence time of $T_2^b=2\,$h. **c**, Energy level diagram for the coupled spins. The spin-polarized alkali-metal atoms, undergoing frequent spin-exchange collisions, can be described as an effective two-level system.

$$\partial_t\begin{pmatrix}\hat{a}\\ \hat{b}\end{pmatrix}=\mathrm{i}\begin{pmatrix}\omega_a+\mathrm{i}\gamma & -J\\ -J & \omega_b\end{pmatrix}\begin{pmatrix}\hat{a}\\ \hat{b}\end{pmatrix}+\hat{\mathbf{f}}. \quad (1)$$

Here ω_a and ω_b denote the Larmor precession frequencies of the collective spins of the alkali-metal and noble-gas atoms, respectively. They are set by the external magnetic field B and by the effective magnetic fields exerted by each species on the other[32]. We tune B to determine the detuning from resonant coupling $\Delta=\omega_a-\omega_b$. The decoherence rate of the alkali-metal excitations γ is included, while for now we neglect the slow decoherence of the noble-gas spins. Finally, $\hat{\mathbf{f}}$ denotes the quantum noise accompanying the relaxation, motion and collision processes[22,24]. In the current study, $\hat{\mathbf{f}}$ can be discarded, as we prepare the spin ensembles in coherent spin states and study the evolution of the mean transverse amplitudes $\langle\hat{a}\rangle$ and $\langle\hat{b}\rangle$.

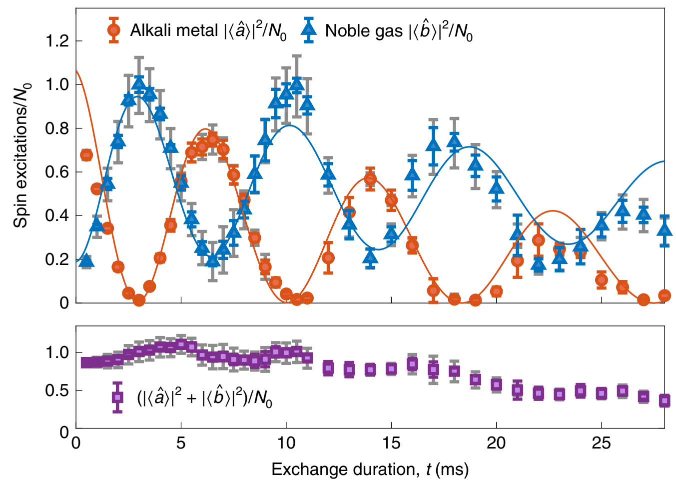

Fig. 2 | Exchange of collective spin excitations. Top: measurement of the coherent exchange between the alkali-metal spin $\langle\hat{a}\rangle$ (red circles) and the noble-gas spin $\langle\hat{b}\rangle$ (blue triangles) in the strong-coupling regime. A short pulse of transverse magnetic field at $t=0$ excites $N_0=|\langle\hat{a}(0)\rangle|^2+|\langle\hat{b}(0)\rangle|^2=(13.2\pm0.6)\times10^{13}$ spins. The experimental conditions at $t=0$ are $J=78\pm8\,$Hz, $\gamma=7.3\pm1.5\,$Hz and $\Delta=-1.15J$ (for obtaining maximal extinction of $\langle\hat{a}\rangle$ at the minima, see text). Lines present the result of a detailed model using these parameters, obtained from independent measurements. Each data point is averaged over 12–20 repetitions of the experimental sequence (Extended Data Fig. 3). Coloured error bars include uncertainties in the spin-projection measurements and the scattering between repetitions. Grey error bars indicate uncertainty due to the uncertainty in the alkali-metal polarization $p_a(t)$, required for converting spin projections to excitations. Bottom: same data in terms of $|\langle\hat{a}\rangle|^2+|\langle\hat{b}\rangle|^2$, confirming that the total number of excitations is conserved by the exchange process, up to an overall decoherence.

Results

Experimental setup and protocols. We study transverse spin excitations of spin-polarized potassium vapour and helium-3 gas enclosed in a spherical glass cell (Fig. 1a). The potassium spins are polarized along the axial magnetic field by an optical pumping beam, and the helium spins are polarized by collisions with the spin-polarized potassium (over 10 h; Extended Data Fig. 1). The cell also contains nitrogen for reducing (quenching) the fluorescence from the optically excited potassium atoms. At low polarization, the helium spins exhibit a coherence time of $T_2^b=2\,$h (Fig. 1b), and consequently their individual relaxation is henceforth neglected. The exchange experiments start with turning off the pumping beam.

We monitor the dynamics of the coupled spin system following a short, 5-μs-long pulse of transverse magnetic field $B_\perp$, which predominantly excites the collective alkali-metal spin and initializes it at a tilt angle of a few degrees from the axial magnetic field $B\hat{\mathbf{z}}$. We measure the transverse alkali-metal spin using Faraday rotation of an optically detuned, linearly polarized probe beam. In this system, the exchange rate J and the magnetic precession rates ω_a and ω_b are all of the same scale when $\Delta\lesssim J$. As a result, strongly coupled dynamics measured in the laboratory frame mixes the effects of Larmor precession with that of the exchange. To eliminate the effect of the former and witness the exchange dynamics directly, we experimentally reconstruct the complex quantities $\langle\hat{a}\rangle$ and $\langle\hat{b}\rangle$, each composed of the two spin components (quadratures) in the transverse x–y plane. The tomographic-like reconstruction is performed by repeated measurements of the alkali-metal spin dynamics in the x–y plane using alternating pulses $B_\perp\hat{\mathbf{y}}$ and $B_\perp\hat{\mathbf{x}}$ for the initial tilt. We properly scale these measurements by the total degree of polarization $p_a(t)$ (measured independently; Extended Data Fig. 2) and

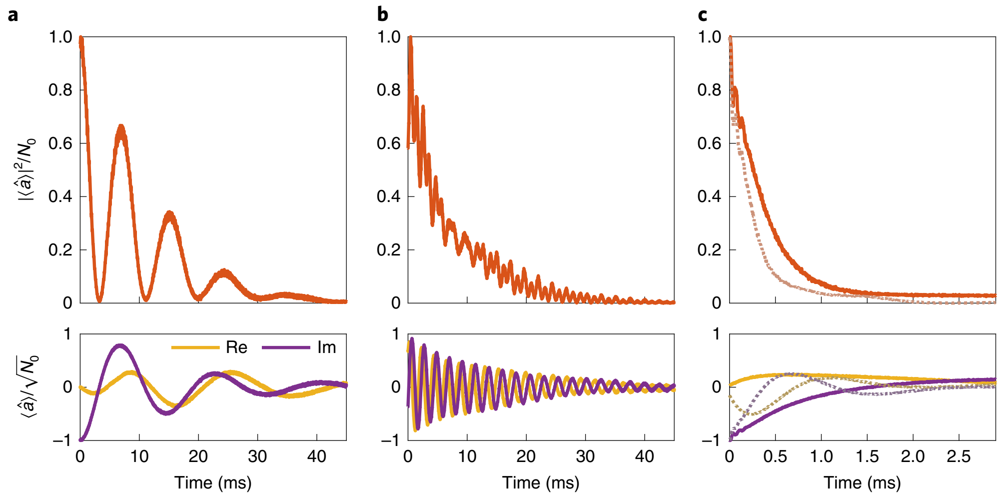

Fig. 3 | Measured dynamics of the coupled alkali-metal–noble-gas spin system in three regimes. All measurements begin with a short magnetic stimulation of $N_0=(5.9\pm0.4)\times10^{13}$ alkali-metal spin excitations, and the initial alkali-metal–noble-gas coupling rate is $J\approx68$ Hz. Top: collective spin excitations of the alkali-metal atoms. Bottom: real and imaginary parts of the collective spin amplitude, associated with the two transverse spin components in the laboratory frame, exhibiting Larmor precession in addition to the exchange. **a**, Strong coupling, achieved when J exceeds the alkali-metal relaxation rate $\gamma=0.11J$ and close to resonance $\Delta=-1.15J$. Recurring collapse and revival of alkali-metal spin excitations provide evidence for a coherent hybridization with the noble-gas spins. **b**, Decoupled dynamics, observed when increasing the detuning to $\Delta=6.8J=66\gamma$ by increasing the magnetic field. The alkali-metal spin, here largely decoupled from the noble-gas spin, undergoes standard Larmor precession and relaxation. **c**, Overdamped dynamics, obtained at $\gamma=3.2J$. When near resonance (solid line, $\Delta=-0.15\gamma$), the long-lived noble-gas spin partially hybridizes with the alkali-metal spin, whose relaxation slows down compared with the non-resonant case (dotted line, $\Delta=\gamma$).

calculate the complex amplitude of the collective alkali-metal spin $\langle\hat{a}(t)\rangle$. To measure the collective noble-gas spin $\langle\hat{b}(t)\rangle$ after some exchange duration t, we halt the exchange dynamics at t by rapidly ramping up the axial magnetic field (increasing Δ) and utilizing the alkali-metal spins as a magnetometer for sensing the noble-gas spin precession.

We realize a maximal coupling rate of $J=78\pm8$ Hz by operating at high densities of potassium $n_a=4.9\times10^{14}\,\mathrm{cm}^{-3}$ (at $T=230\,°\mathrm{C}$) and helium $n_b=6.45\times10^{19}\,\mathrm{cm}^{-3}$ (2.4 atm at room temperature) and with relatively high degrees of spin polarization $p_a\gtrsim0.95$ and $p_b\gtrsim0.3$. At these conditions, collisions among alkali-metal atoms are frequent enough ($>0.5\,\mu\mathrm{s}^{-1}$) with respect to the Larmor frequency to keep the alkali-metal excitations free from spin-exchange relaxation[32]. The intricate hyperfine manifold of the alkali-metal atoms maintains a spin-temperature distribution due to these collisions and manifests as an effective spin-1/2 (Fig. 1c)[32]. Remnant spin relaxation occurring during these collisions dominates the decoherence rate of the alkali-metal excitations $\gamma=7.3\pm1.5$ Hz. We thus achieve $J\gtrsim10\gamma$. See Methods for a detailed description of the experimental conditions and analysis procedures.

Dynamics of strongly coupled spins. Under the strong-coupling conditions, the two spin gases can coherently exchange collective excitations. To demonstrate these dynamics, we tune Δ close to resonance and generate an initial excitation predominantly of the alkali-metal spin. Figure 2 presents the measured spin excitations $|\langle\hat{a}\rangle|^2$ and $|\langle\hat{b}\rangle|^2$ as they are exchanged back and forth between the two ensembles. Because the magnetic pulse acts also on the noble-gas spin and partially excites it as well, the extinction of $|\langle\hat{a}(t)\rangle|^2$ at the minima of the observed oscillations is maximized slightly below resonance, at $\Delta=-1.15J$. The presented measurement is taken at this detuning. This detuning is still small in terms of the strong-coupling dynamics, rendering a near-unity ratio between the exchange and coupling rates $\tilde{J}/J=1.15$, where $\tilde{J}\approx\sqrt{J^2+\Delta^2/4}$ is the exchange rate. We observe the reversible exchange and the revival of the excitations back to the alkali-metal spins at $t=6.5$ ms and with a high contrast of 75%, evidencing the strongly coupled dynamics. The uncertainty on the exchange fidelity is small (7.4%) for short exchange times, and it is dominated by uncertainty in the alkali-metal axial polarization (Methods).

As expected, we find that the exchange conserves the total number of excitations $|\langle\hat{a}\rangle|^2+|\langle\hat{b}\rangle|^2$ aside from the decay introduced by alkali-metal spin decoherence. We also directly observe the slowing down of the exchange oscillations, as the spins gradually decouple due to the dependence of J on the decaying alkali-metal polarization $p_a(t)$. The gradual decoupling leads to residual excitations populating the long-lived noble-gas spin. These effects are all captured by a detailed model (solid lines; Methods), which accounts for the temporal decrease of J and for small geometric misalignments.

Coupling regimes. It is instructive at this point to compare the resonant, strong-coupling dynamics with the detuned and overdamped dynamics. These are presented in Fig. 3, showing the measured total number $|\langle\hat{a}\rangle|^2$ of collective alkali-metal spin excitations (top) and the amplitudes $\mathrm{Re}\langle\hat{a}\rangle$ and $\mathrm{Im}\langle\hat{a}\rangle$, which exhibit also Larmor precession (bottom). For the coherent spin states in our experiment, oscillations of $|\langle\hat{a}(t)\rangle|^2$ correspond to nutations (tilt) of the collective alkali-metal spin from the quantization axis $\hat{\mathbf{z}}$ and therefore manifest the exchange interaction in a rotating frame, free of Larmor precession in the x–y plane.

First, we set Δ close to resonance ($\Delta=-1.15J$ as before) and measure the dynamics under the strong-coupling conditions $J=68\pm5$ Hz and $\gamma=7.5\pm2$ Hz (Fig. 3a). As in Fig. 2, we observe oscillations of the number of alkali-metal spin excitations $|\langle\hat{a}(t)\rangle|^2$, exchanged back and forth with the noble-gas spin while gradually decaying. The dynamics far off-resonance is shown for an increased detuning $\Delta=460\,\mathrm{Hz}\approx6.8J$ (Fig. 3b). In this regime, we observe a decaying precession of $\langle\hat{a}(t)\rangle$ and an almost monotonic relaxation of $|\langle\hat{a}(t)\rangle|^2$ at a rate 14 ± 2 Hz, in agreement with the expected value (2γ). Finally, we repeat the experiments with an increased relaxation rate $\gamma=215\,\mathrm{Hz}\approx3.2J$ (Fig. 3c), implemented by keeping the pumping beam on during the measurement. The measurements shown

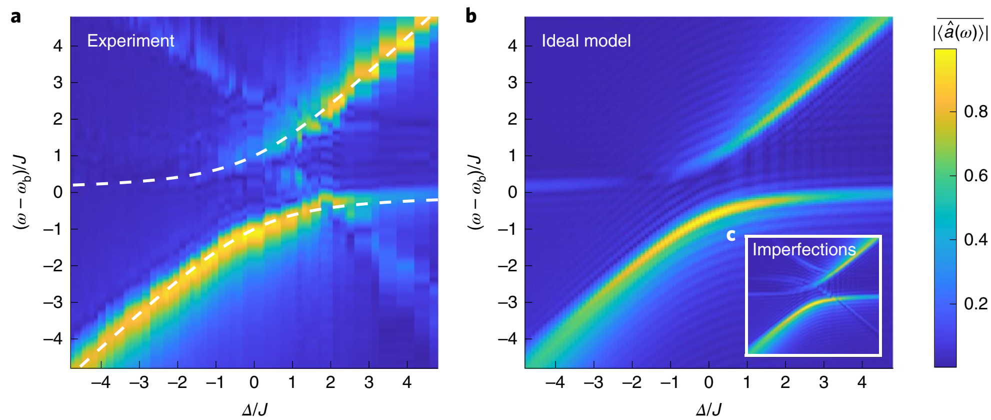

Fig. 4 | Spectral response of the alkali-metal–noble-gas spin system in the strong-coupling regime. a, Measured response of the collective alkali-metal spin $\langle \hat{a} \rangle$ to a weak stimulation, for different detunings between the spins Δ. The spectrum $\overline{\langle \hat{a}(\omega) \rangle} \propto \int_0^\infty \langle \hat{a}(t) \rangle e^{-i\omega t}\, dt$ (normalized separately for each Δ; Methods) manifests the eigenvalues of the coupled system. The spectrum maxima correspond to the normal frequencies, and the spectral widths are indicative of the decay. Dashed lines present the imaginary part of the eigenvalues of equation (1). A clear avoided crossing with a sizeable spectral gap at $|\Delta| < J$ indicates the strong, coherent hybridization of the two spin gases. The response at $|\Delta| > J$ corresponds to the independent precession rates of the alkali-metal and noble-gas spins ω_a and ω_b, respectively. The axes are scaled by the average value $J = 47$ Hz (rather than the initial value $J = 78$ Hz) to account for the decrease of J due to alkali-metal depolarization during the 65-ms-long measurement. The frequency axis is shifted by $\omega_b = 42.9$ Hz. **b**, Spectral response calculated from a detailed model. **c**, An experimental misalignment of 4.4 mrad between the magnetic field and the pumping direction, when added to the calculation, reproduces the weak perpendicular branches.

in Fig. 3 of the three regimes elucidate the coherent nature of the exchange interaction under the strong-coupling conditions.

The transition between the overdamped and strong-coupling regimes is continuous, with the reversible dynamics becoming gradually more dominant. At critical damping $J = \gamma/2$, the decay of the alkali-metal spin is shared among both species, and its coherence time is effectively elongated. Figure 3c demonstrates the elongation for on-resonance dynamics (solid) compared with the detuned case (dotted). While $J/\gamma > 0.5$ promotes an avoided crossing of the normal frequencies of the dynamics (as discussed below), the reversible exchange is negligible at critical damping. At $J/\gamma = 0.78$, for example, as realized by Kornack and Romalis[3], only 0.5% of the initial excitations return to the initially tilted gas (Supplementary Section 2). Efficient and reversible exchange of excitations, therefore, requires the ratio J/γ to be large.

Spectral map. At strong coupling, the system's response to magnetic fields features a spectral gap. We measure this gap by repeating the experiment presented in Fig. 3a for different values of Δ. The spectral map (Fig. 4a) reveals an avoided crossing between the normal frequencies at $\Delta = 0$, with a wide gap indicating a strong coherent coupling between the two gases. We further compare the measurements with calculated spectra. We present both a simple model based on equation (1) (Fig. 4a, dashed lines) and the results of the detailed model (Fig. 4b,c). Both models reproduce well the main frequency branches. The additional features in the spectrum, primarily the weak perpendicular branches and the vanishing amplitude of the horizontal branch at $\Delta \gtrsim J$ (due to reduced sensitivity to magnetic stimulation near the so-called compensation point[3]), are well captured by the detailed model.

Discussion

We realize strong coherent coupling between the collective spins of a dense alkali-metal vapour and a noble gas, with a coupling-to-decay ratio $J/\gamma \approx 10.7$, much larger than unity. The coupling arises from accumulation of stochastic spin-exchange collisions, relying on the weakness of each collision (spin precession of $\sim 10^{-5}$ rad per collision) to conserve coherence and reversibility[22]. We estimate that higher values of J/γ are achievable with higher ^{3}He density and polarization and at lower temperatures and nitrogen gas pressure. ^{3}He pressure exceeding 10 atm was demonstrated[1] as well as 85% polarization[36]. A system at 220 °C, with 8.2 atm of ^{3}He polarized to 80% and near-unity polarized potassium is expected to reach $J/\gamma > 100$.

Operation of alkali-metal and noble-gas systems in the strong-coupling regime opens several intriguing possibilities. One route motivated by quantum information applications is to use the alkali-metal spins as mediators between photons and noble-gas spins[18,35]. In particular, fast on-resonance coupling between the spins can enhance the indirect coupling to photons and improve the performance of these applications compared with detuned operation. At strong coupling, read-in, read-out and control of the collective noble-gas spin are done at a rate J, whereas detuned operations with $\Delta \gg J$ are done at a substantially lower rate J^2/Δ (up to Hz scale). The efficiency and fidelity of the operation are application dependent and could be optimal in either of the two regimes. For long-lived optical quantum memories, the optimal regime depends on the bandwidth B of the optical signal[18]. In systems with $J \gtrsim \gamma$, storage of photons with an optical bandwidth $B \gg \gamma$ (kHz up to GHz) is optimized by first storing the light on the alkali-metal spins and then transferring it to the noble-gas spins via a strong coupling exchange. The exchange efficiency, approximately $\exp(-\pi\gamma/2J)$, approaches unity for $J \gg \gamma$ and could enable hours-long storage with unprecedented time–bandwidth product. Another example relates to the generation of long-lived spin entanglement between multiple cells via detuned operation[5]. Once the entanglement is generated, efficient extraction for subsequent usage requires transfer to the alkali-metal spins, which would rely on strongly coupled exchange. Furthermore, for $J \gg \gamma$, the generation is more efficient regardless of the detuning, as the contribution of alkali-metal projection noise is suppressed by a factor $4\gamma B/J^2$, where B^{-1} is the duration of the entangling pulse.

A second potential route is to use the strong coupling for improving noble-gas-based sensors. Noble-gas magnetometers sense magnetic fields by measuring the precession of noble-gas spins with an additional auxiliary magnetometer. They are particularly interesting, being fundamentally limited by the low noble-gas projection noise[1].

Using the alkali-metal spin as an embedded magnetometer enables suppression of its projection-noise contribution by a large factor over the projection noise of the noble gas when $J \gg \sqrt{\gamma/T_2^{\mathrm{b}}}$ (ref. [22]). In addition, operation in the strong-coupling regime outperforms detuned operations in two aspects. First, detuned operation reduces the magnetic sensitivity at low frequencies near the nuclear magnetic resonance frequency of the noble gas, effectively increasing the impact of photon shot noise. Second, bringing the two spins to a resonance implies lowering the alkali-metal precession frequency, which in turn enables operation in the spin-exchange relaxation-free regime where sensitivity is increased even further[32,37]. Finally, another application regards self-compensating magnetometers, which typically operate on resonance[13,16]. These sensors can readily benefit from an enhanced coupling rate, which could provide for higher bandwidth and dynamic range.

Online content

Any methods, additional references, Nature Research reporting summaries, source data, extended data, supplementary information, acknowledgements, peer review information; details of author contributions and competing interests; and statements of data and code availability are available at https://doi.org/10.1038/s41567-022-01535-w.

Received: 9 February 2021; Accepted: 4 February 2022;
Published online: 4 April 2022

References

1. Gentile, T. R., Nacher, P. J., Saam, B. & Walker, T. G. Optically polarized ^{3}He. *Rev. Mod. Phys.* **89**, 045004 (2017).
2. Walker, T. G. & Larsen, M. S. Spin-exchange-pumped NMR gyros. *Adv. Atom. Mol. Opt. Phys.* **65**, 373 (2016).
3. Kornack, T. W. & Romalis, M. V. Dynamics of two overlapping spin ensembles interacting by spin exchange. *Phys. Rev. Lett.* **89**, 253002 (2002).
4. Jimenez-Martinez, R. et al. Optical hyperpolarization and NMR detection of ^{129}Xe on a microfluidic chip. *Nat. Commun.* **5**, 3908 (2014).
5. Katz.O., Shaham, R., Polzik, E. S. & Firstenberg, O. Long-lived entanglement generation of nuclear spins using coherent light. *Phys. Rev. Lett.* **124**, 043602 (2020).
6. Katz, O., Reches, E., Shaham, R., Gorshkov, A. V. & Firstenberg, O. Optical quantum memory with optically inaccessible noble-gas spins. Preprint at https://arxiv.org/abs/2007.08770 (2020).
7. Heil, W. et al. Spin clocks: probing fundamental symmetries in nature. *Ann. Phys.* **525**, 539–549 (2013).
8. Gemmel, C. et al. Ultra-sensitive magnetometry based on free precession of nuclear spins. *Eur. Phys. J. D* **57**, 303–320 (2010).
9. Kornack, T. W., Ghosh, R. K. & Romalis, M. V. Nuclear spin gyroscope based on an atomic comagnetometer. *Phys. Rev. Lett.* **95**, 230801 (2005).
10. Thrasher, D. A. et al. Continuous comagnetometry using transversely polarized Xe isotopes. *Phys. Rev. A* **100**, 061403 (2019).
11. Kitching, J. Chip-scale atomic devices. *Appl. Phys. Rev.* **5**, 031302 (2018).
12. Chupp, T. & Swanson, S. Medical imaging with laser-polarized noble gases. *Adv. Atom. Mol. Opt. Phys.* **45**, 41–98 (2001).
13. Brown, J. M., Smullin, S. J., Kornack, T. W. & Romalis, M. V. New limit on Lorentz- and CPT-violating neutron spin interactions. *Phys. Rev. Lett.* **105**, 151604 (2010).
14. Jackson Kimball, D. F., Boyd, A. & Budker, D. Constraints on anomalous spin–spin interactions from spin-exchange collisions. *Phys. Rev. A* **82**, 062714 (2010).
15. Alonso, R., Blas, D. & Wolf, P. Exploring the ultra-light to sub-MeV dark matter window with atomic clocks and co-magnetometers. *J. High Energy Phys.* **2019**, 69 (2019).
16. Bloch, I. M., Hochberg, Y., Kuflik, E. & Volansky, T. Axion-like relics: new constraints from old comagnetometer data. *J. High Energy Phys.* **2020**, 167 (2020).
17. Chupp, T. E., Fierlinger, P., Ramsey-Musolf, M. J. & Singh, J. T. Electric dipole moments of atoms, molecules, nuclei, and particles. *Rev. Mod. Phys.* **91**, 015001 (2019).
18. Katz, O., Shaham, R., Reches, E., Gorshkov, A. V. & Firstenberg, O. Optimal control of an optical quantum memory based on noble-gas spins. Preprint at https://arxiv.org/abs/2007.10177 (2020).
19. Dantan, A. et al. Long-lived quantum memory with nuclear atomic spins. *Phys. Rev. Lett.* **95**, 123002 (2005).
20. Serafin, A., Fadel, M., Treutlein, P. & Sinatra, A. Nuclear spin squeezing in helium-3 by continuous quantum nondemolition measurement. *Phys. Rev. Lett.* **127**, 013601 (2021).
21. Serafin, A., Castin, Y., Fadel, M., Treutlein, P. & Sinatra, A. Étude théorique de la compression de spin nucléaire par mesure quantique non destructive en continu. *C. R. Phys.* **22**, 1–35 (2021).
22. Katz, O., Shaham, R. & Firstenberg, O. Quantum interface for noble-gas spins. *PRX Quantum* **3**, 010305 (2022).
23. Hammerer, K., Sorensen, A. S. & Polzik, E. S. Quantum interface between light and atomic ensembles. *Rev. Mod. Phys.* **82**, 1041–1093 (2010).
24. Shaham, R., Katz, O. & Firstenberg, O. Quantum dynamics of collective spin states in a thermal gas. *Phys. Rev. A* **102**, 012822 (2020).
25. Sun, J. et al. Spatial multiplexing of squeezed light by coherence diffusion. *Phys. Rev. Lett.* **123**, 203604 (2019).
26. Dellis, A. T., Loulakis, M. & Kominis, I. K. Spin-noise correlations and spin-noise exchange driven by low-field spin-exchange collisions. *Phys. Rev. A* **90**, 032705 (2014).
27. Kong, J. Measurement-induced, spatially-extended entanglement in a hot, strongly-interacting atomic system. *Nat. Commun.* **11**, 2415 (2020).
28. Mouloudakis, K. & Kominis, I. K. Spin-exchange collisions in hot vapors creating and sustaining bipartite entanglement. *Phys. Rev. A* **103**, L010401 (2021).
29. Sherson, J. F. et al. Quantum teleportation between light and matter. *Nature* **443**, 557–560 (2006).
30. Gorshkov, A. V., Andre, A., Fleischhauer, M., Sorensen, A. S. & Lukin, M. D. Universal approach to optimal photon storage in atomic media. *Phys. Rev. Lett.* **98**, 123601 (2007).
31. Firstenberg, O. et al. Self-similar modes of coherent diffusion. *Phys. Rev. Lett.* **105**, 183602 (2010).
32. Appelt, S. et al. Theory of spin-exchange optical pumping of ^{3}He and ^{129}Xe. *Phys. Rev. A* **58**, 1412–1439 (1998).
33. Batz, M., Nacher, P. J. & Tastevin, G. Fundamentals of metastability exchange optical pumping in helium. *J. Phys. Conf. Ser.* 294, 012002 (2011).
34. Walter, D. K., Happer, W. & Walker, T. G. Estimates of the relative magnitudes of the isotropic and anisotropic magnetic-dipole hyperfine interactions in alkali-metal-noble-gas systems. *Phys. Rev. A* **58**, 3642–3653 (1998).
35. Katz, O., Shaham, R. & Firstenberg, O. Coupling light to a nuclear spin gas with a two-photon linewidth of five millihertz. *Sci. Adv.* **7**, eabe9164 (2021).
36. Chen, W. C., Gentile, T. R., Ye, Q., Walker, T. G. & Babcock, E. On the limits of spin-exchange optical pumping of 3He. *J. Appl. Phys.* **116**, 014903 (2014).
37. Allred, J. C., Lyman, R. N., Kornack, T. W. & Romalis, M. V. High-sensitivity atomic magnetometer unaffected by spin-exchange relaxation. *Phys. Rev. Lett.* **89**, 130801 (2002).

Methods

Holstein–Primakoff transformation from spins to bosonic excitations. The states of the alkali-metal and noble-gas spin ensembles are characterized by their degree of polarization $p_a = (2/N_a)\langle\sum_m \hat{s}_z^{(m)}\rangle$ and $p_b = (2/N_b)\langle\sum_n \hat{k}_z^{(n)}\rangle$. Here $\sum_m \hat{s}_j^{(m)}$ and $\sum_n \hat{k}_j^{(n)}$ with $j=\{x,y,z,-,+\}$ are the standard collective spin operators of the electrons of the alkali-metal atoms and the nuclei of the noble-gas atoms, respectively, and $N_a = n_a V$ and $N_b = n_b V$ are the number of atoms in the volume V. Describing the alkali-metal spins in terms of only the electronic spins is possible owing to the frequent alkali-metal–alkali-metal collisions, which constantly drive the alkali-metal atoms to a spin-temperature distribution[38]. In the spin-temperature distribution, due to the hyperfine coupling to the alkali-metal nuclear spin, the spin precession around an external magnetic field is slower than that of a bare electron by a factor $q(p_a)$, known as the slowing-down factor. For potassium, $q(p_a) = 2 + 4/(1+p_a^2)$ (refs. [37–39]).

We are interested in the bosonic annihilation operators $\hat{a}$ and $\hat{b}$, defined according to the Holstein–Primakoff transformation as $\hat{a} = \sqrt{q/N_a p_a}\sum_m \hat{s}_-^{(m)}$ and $\hat{b} = \sqrt{1/N_b p_b}\sum_n \hat{k}_-^{(n)}$ (refs. [22,23]). These are the canonical, normalized version of the collective spin operators transverse to the quantization axis. For the alkali-metal spins, we denote the homogeneous depolarization rate by $\Gamma_p = -(\partial_t p_a)/p_a$ and the transverse relaxation rate by $\Gamma_2 = \Gamma_c + \Gamma_p$ (the decay rate of $\langle\sum_m \hat{s}_x^{(m)}\rangle$ and $\langle\sum_m \hat{s}_y^{(m)}\rangle$), where Γ_c is the dephasing rate. The decoherence rate of the excitations $\langle\hat{a}\rangle$ is therefore given by $\gamma = \Gamma_c + \Gamma_p/2$, neglecting small variations of q on short timescales. The noise on $\langle\hat{a}\rangle$ (technical or fundamental) signifies incoherent excitations, which inevitably increase when the polarization decays. As a result, the process of depolarization ($\Gamma_p > 0$), while contributing only partially ($\Gamma_p/2$) to the collective excitations decoherence, contributes as well to the increase of the fundamental and technical noises. In the Supplementary Information, we derive formal expressions for the decay and noise, describe the temporal dynamics of non-classical states in the Heisenberg–Langevin formalism and demonstrate the growth of quantum uncertainty due to spin depolarization for a squeezed coherent state.

Apparatus and experimental conditions. We use a spherical cell with diameter $\ell = 2.54$ cm and volume $V = 8.6\,\mathrm{cm}^3$, made of GE-180 aluminosilicate glass, containing ^{3}He gas, a droplet of natural abundant potassium and 50 Torr of nitrogen. The temperature of the cell $T = 230$ °C is maintained using a pair of twisted resistance wires wrapped around an alumina body, which are driven with a current oscillating at 320 kHz. The magnetic field is applied via three sets of coils: four-winding double Helmholtz coils for controlling $B\hat{\mathbf{z}}$ and a bird-cage coil for the transverse fields to improve the magnetic uniformity. The coils are placed inside five concentric layers of μ-metal magnetic shields, and the inner two layers are degaussed.

The $N_a = 4.2\times10^{15}$ potassium atoms are polarized by optical pumping using 500 mW of circularly polarized light at 770 nm. This pumping light is generated using a free-running diode laser followed by a tapered amplifier. We tune the laser near the optical D1 transition, which in our setup appears as a single absorption line with a full width of 32 GHz due to pressure broadening, producing an on-resonance optical depth of $n_a\sigma_{abs}\ell \approx 220$ (where $\sigma_{abs} = 1.76\times10^{-13}\,\mathrm{cm}^2$ is the absorption cross-section of the 32-GHz-wide line). The pumping beam is Gaussian with a 25 mm waist diameter. We detune it from resonance to reduce its depletion and achieve a high degree of spin polarization $p_a \geq 0.95$.

Spin-destruction collisions among potassium atoms and the spin-rotation interaction of potassium atoms with the buffer gas dominate the depolarization of the potassium spins in the dark[40]. The depolarization is generally a multi-exponential process (Extended Data Fig. 2b), and yet, at short times, it can be described by the single rate $\Gamma_p = 11.4$ Hz. Rapid spin-exchange collisions among potassium atoms at a rate $R_{se} = 86$ kHz and the operation at low Larmor precession rates $|\omega_a| \ll \sqrt{R_{se}\Gamma_p}$ put the potassium in the so-called spin-exchange relaxation-free regime[37,41], rendering the relaxation induced by spin-exchange collisions between pairs of alkali-metal atoms negligible. Consequently, the transverse spin relaxation rate $\Gamma_2 = \Gamma_p + \Gamma_c = 13$ Hz is dominated by the depolarization processes, with a minor contribution from magnetic inhomogeneity ($\Gamma_c = 1.6$ Hz). These lead to a decoherence rate of $\gamma = \Gamma_c + \Gamma_p/2 \approx 7.3$ Hz for the bosonic excitations of the collective potassium spin.

The $N_b = 5.5\times10^{20}$ helium atoms are hyperpolarized using spin-exchange optical pumping (SEOP)[38] at a rate of 3.6×10^{-6} Hz in the presence of an axial magnetic field $B = 400$ mG. A typical SEOP measurement settling at $p_b \geq 0.3$ is presented in Extended Data Fig. 1. In our system, at low temperature, the measured depolarization and decoherence times of the helium spins $T_1^b = 22$ h and $T_2^b = 2$ h are limited by magnetic field inhomogeneity within the cell volume. At elevated temperature and polarizations, we measure $T_{1,\mathrm{act}}^b = 3.9$ h (Extended Data Fig. 1) dominated by the inhomogeneity of the magnetizations of the two ensembles in the cell, which deviates slightly from an ideal sphere[42]. To moderate the helium depolarization during the experiments, we intermittently turn on the SEOP in between measurements.

The polarized spin ensembles exert an equivalent magnetic field on each other, via collisions and via the macroscopic magnetic fields generated by their magnetization. While the equivalent magnetic field experienced by the helium $B_{a\to b} = -0.24$ mG (for $p_a = 0.98$) is small, the equivalent magnetic field experienced by the potassium $B_{b\to a} = -10.94$ mG (for $p_b = 0.3$) is considerable. The detuning from resonant coupling Δ is thus quite sensitive to p_b, which we monitor during the experiment. We do so by applying a constant magnetic field $-B_{b\to a} + 1.6$ mG, and monitoring the precession frequency of the decoupled alkali-metal spins following a small transverse magnetic pulse.

In the experiments presented in Figs. 2–4, we use a transverse magnetic pulse to tilt the alkali-metal spins by $\theta_a = 9.8 \pm 0.2°$, $\theta_a = 6.8 \pm 0.2°$ and $\theta_a = 0.7 \pm 0.05°$, respectively. In terms of the number of excitations $|\langle\hat{a}\rangle|^2 = qN_a p_a\theta_a^2/4$, these correspond to $|\langle\hat{a}\rangle|^2 = (12.1 \pm 0.5)\times10^{13}$, $|\langle\hat{a}\rangle|^2 = (5.9 \pm 0.4)\times10^{13}$ and $|\langle\hat{a}\rangle|^2 = (6.2 \pm 0.9)\times10^{11}$.

In all experiments, we measure the transverse spin component of the alkali-metal atoms along the $\hat{\mathbf{x}}$ axis using Faraday rotation of a linearly polarized probe beam. The 5 mm diameter, 260 μW probe beam is detuned by ~400 GHz above the D1 transition, and its polarization is measured after the cell using the balanced photodetection method[43]. We subtract from all measurements a background signal taken without the magnetic pulse. This background signal is small and is dominated by excitations of transverse spins during the fast variation of $B\hat{\mathbf{z}}$ (when setting Δ) because of the imperfect alignment between the optical and magnetic axes.

Reconstruction and scaling of $\langle\hat{a}\rangle$ and $\langle\hat{b}\rangle$. We use optical Faraday rotation to measure $\langle\hat{a}\rangle$ and $\langle\hat{b}\rangle$. For the optically broadened line and the far-detuned probe in our setup, and as long as the Faraday rotation angle is small, the balanced-detection readout is proportional to the $\hat{\mathbf{x}}$ component of the collective alkali-metal spin $\langle\sum_m \hat{s}_x^{(m)}\rangle$, that is, to the electron spin projection along the probing axis[44]. From these measurements, we extract the normalized transverse spin component $\bar{S}_x(t) = \langle\sum_m \hat{s}_x^{(m)}(t)\rangle/[N_a p_a(0)/2]$. The normalization factor is calibrated separately by tilting the initial spin $[N_a p_a(0)/2]\hat{\mathbf{z}}$ all the way to the $\hat{\mathbf{x}}$ direction (equivalent to $\theta_a = 90°$) and measuring the maximal Faraday rotation angle (~4 rad in our system). We verify that the Faraday rotation angle in all subsequent experiments is small.

The measurements of $|\langle\hat{a}(t)\rangle|^2$ and $|\langle\hat{b}(t)\rangle|^2$ presented in Fig. 2 are done according to the experimental sequence shown in Extended Data Fig. 3a. The sequence starts by initializing the spins with a small transverse component under conditions of small Δ. After some evolution and partial decay in the dark, at time t, we increase Δ by an order of magnitude (by increasing $B + B_{b\to a}$ to 1.5 mG), thus largely decoupling the alkali-metal and noble-gas spins. We continue to monitor the alkali-metal spins and use them as a magnetometer for sensing the noble-gas spins.

During the experiment, when the pumping light is off, the polarization of the alkali-metal spin decays $p_a(t) \leq p_a(0)$. This decay changes the slowing-down factor $q(t) = q[p_a(t)]$ and thus shifts the Larmor precession frequency of the alkali-metal spin, which we measure directly (Extended Data Fig. 2a). We model the time dependence of the shift, assuming an exponential polarization decay $\partial_\tau p_a = -\tilde{\Gamma}_p p_a$, where τ is the time elapsed from the decoupling time t and $\tilde{\Gamma}_p$ is the depolarization rate at the increased magnetic field. The instantaneous precession frequency of the alkali-metal spin is then given by

$$\omega_a(\omega_0, p_a(t), \tilde{\Gamma}_p; \tau) = \frac{2\omega_0}{1 + 2/[1 + p_a^2(t)e^{-2\tilde{\Gamma}_p\tau}]}, \tag{2}$$

where $\omega_0 = \omega_a(p_a = 1; \tau = 0)$. To each measured signal $\bar{S}_x$, we therefore fit the model

$$\bar{S}_x(t+\tau) = \mathrm{Re}\left[\sigma_a(t)e^{i\int_0^\tau \omega_a(\omega_0, p_a(t), \tilde{\Gamma}_p; \tau')d\tau' - \gamma_a\tau} + \sigma_b(t)e^{(i\omega_b - \gamma_b)\tau}\right]. \tag{3}$$

Here $\sigma_a(t)$ and $\sigma_b(t)$ are complex fitting parameters, corresponding to the amplitudes of the two frequency components, and γ_a, γ_b, ω_0, ω_b and $p_a(t)$ are real fitting parameters. One such fit is demonstrated in Extended Data Fig. 3b, and the extracted $p_a(t)$, $\omega_a(t, \tau = 0)$, $|\sigma_a(t)|^2$ and $|\sigma_b(t)|^2$ are shown in Extended Data Fig. 2b (note the factor $|\sigma_b/\sigma_a|^2 \approx (J/\Delta)^2 < 1/100$). We verify that the extracted amplitudes are insensitive to the exact value of $\tilde{\Gamma}_p$ (set to be 8.6 Hz in all fits) and even to the functional form of $p_a(t+\tau)$. We use the fits to extract $p_a(t)$ (Extended Data Fig. 2b) and find that it is accurately described by the double-exponent function $p_a(t) = 0.61e^{-t/(9.1\,\mathrm{ms})} + 0.381e^{-t/(102\,\mathrm{ms})}$, presented in Extended Data Fig. 2b with its confidence bounds. The multi-exponential nature of the depolarization can be attributed to multi-mode spatial dynamics[24], to SEOP of the alkali metal by the noble gas and to low signal-to-noise ratios.

With $p_a(t)$ at hand, we obtain the factor $\eta(t) = \frac{N_a q[p_a(t)]p_a^2(0)}{4p_a(t)}$ between the number of alkali-metal excitations and $\bar{S}_x^2$. The alkali-metal and noble-gas excitations presented in Fig. 2 are then given by $|\langle\hat{a}(t)\rangle|^2 = \eta(t)|\sigma_a(t) + \sigma_b(t)|^2$ and $|\langle\hat{b}(t)\rangle|^2 = \eta(t)\left|\frac{\Delta(t)}{J(t)}\sigma_b(t) - \frac{J(t)}{\Delta(t)}\sigma_a(t)\right|^2$, where $\Delta(t) = \omega_a(t, \tau = 0) - \omega_b$ and $J(t) = \sqrt{\frac{p_a(t)}{p_a(0)}\frac{q(0)}{q[p_a(t)]}}J(t = 0)$. These expressions neglect terms of order

$(J/\Delta)^2$ and higher. Here we see that the decay of $p_a(t)$ increases η, justifying the relation $\gamma \leq \Gamma_2$ and explaining the growth of noise in the measurements, which one can interpret as excess thermal excitations. This process leads to the increasing error bars in Fig. 2 at later times. For the experiments presented in Figs. 3 and 4, we reconstruct the complex-valued $\langle \hat{a}(t) \rangle = \sqrt{\eta(t)}[\bar{S}_x(t) - \mathrm{i}\bar{S}_y(t)]$. The two normalized projections $\bar{S}_x(t)$ and $\bar{S}_y(t)$ are measured in two consecutive experiments that differ in the direction of the initial pulsed excitation (alternating between $B_\perp \hat{\mathbf{y}}$ and $B_\perp \hat{\mathbf{x}}$). In Fig. 2, we average consecutive measurements with the two excitation directions. We use the extracted $p_a(t)$ for Fig. 3a,b and estimate $p_a = p_a(t=0) = 0.98$ for Fig. 3c. Finally, in Fig. 4 we present the normalized Fourier amplitudes $|\overline{\langle \hat{a}(\omega) \rangle}| = |\int_0^\infty \langle \hat{a}(t) \rangle e^{-i\omega t} \mathrm{d}t| / \sqrt{T \int_0^\infty |\langle \hat{a}(t) \rangle|^2 \mathrm{d}t}$, where $T = 65$ ms is the sequence duration.

Detailed model. Equation (1) describes the idealized dynamics of the spin gases. For the calculations presented in Figs. 2 and 4b,c, we use a detailed model, which includes the decay of the alkali-metal polarization $p_a = p_a(t)$ during the experimental sequence, the dependence of Δ and J on $p_a(t)$ (both directly and via the slowing-down factor $q[p_a(t)]$), the misalignment of the optical and magnetic axes and the residual transverse magnetic fields.

The model assumes that both spin ensembles are initially polarized along $-\hat{\mathbf{z}}$. It follows refs. [22,38] and describes the dynamics of the collective spin excitations $S_- = \langle \sum_m \hat{s}_-^{(m)} \rangle$ and $K_- = \langle \sum_n \hat{k}_-^{(n)} \rangle$, coupled by the Fermi-contact interaction occurring during collisions. In the presence of the axial magnetic field $B\hat{\mathbf{z}}$ and the transverse magnetic field $B_- = B_x - \mathrm{i}B_y$, the coupled spin equations are given by

$$\begin{aligned} \partial_t S_- &= \mathrm{i}(\omega_a + \mathrm{i}\Gamma_2) S_- - \mathrm{i}\tfrac{n_a}{q n_b} J_a K_- + \mathrm{i}\tfrac{g_e}{q} \tfrac{N_a p_a}{2} B_-, \\ \partial_t K_- &= -\mathrm{i}\tfrac{q n_a}{n_b} J_b S_- + \mathrm{i}\omega_b K_- + \mathrm{i} g_b \tfrac{N_b p_b}{2} B_-. \end{aligned} \tag{4}$$

Here $J_a = \sqrt{q}\tilde{\zeta} n_b p_a/2$ and $J_b = \tilde{\zeta} n_a p_b / 2\sqrt{q}$ are the unidirectional coupling rates, eventually composing the bidirectional rate $J = \sqrt{J_a J_b}$, with $\tilde{\zeta} = (2 \times 10^{-14}\ \mathrm{cm^3\ s^{-1}})/\sqrt{q}$. The gyromagentic ratios of the electron and helium-3 spins are $g_e = -2.8 \times 10^6$ Hz G^{-1} and $g_b = -3.24 \times 10^3$ Hz G^{-1}, and the precession frequencies are $\omega_a = g_e B/q + \tilde{\zeta} n_b p_b / 2\sqrt{q}$ and $\omega_b = g_b B + \sqrt{q}\tilde{\zeta} n_a p_a / 2$.

We simulate the experimental sequences by numerically solving these equations. From the simulation results, we calculate the expectation values $\langle \hat{a} \rangle = \sqrt{q[p_a(t)]/N_a p_a(t)} S_-(t)$ and $\langle \hat{b} \rangle = \sqrt{1/N_b p_b} K_-(t)$. For the model parameters, we use known constants or the measured values from the calibration experiments. We use $p_a(t) = 0.61 e^{-t/(9.1\,\mathrm{ms})} + 0.381 e^{-t/(102\,\mathrm{ms})}$ for the alkali-metal polarization and $p_b = n_a k_{\mathrm{SE}} p_a(0) T_{1,\mathrm{act}}^{\mathrm{b}} = 0.32$ for the noble-gas polarization, where $k_{se} = 5.5 \times 10^{-20}$ cm^3 s^{-1} is the SEOP rate.

The model can account for various geometric misalignments and other experimental imperfections: (1) Misalignment of the pumping beam from the $\hat{\mathbf{z}}$ axis generates an initial transverse spin component. If the pumping beam points towards $\eta_x \mathbf{e}_x + \eta_y \mathbf{e}_y + \mathbf{e}_z$ (given $\eta_{x,y} \ll 1$), the initial value of S_- is $N_a p_a(t=0)(\eta_x - \mathrm{i}\eta_y)/2$. (2) A residual magnetic field pointing towards $\beta_x \mathbf{e}_x + \beta_y \mathbf{e}_y + \mathbf{e}_z$ (given $\beta_{x,y} \ll 1$) during the SEOP process would turn the initial value of K_- to $N_b p_b (\beta_x - \mathrm{i}\beta_y)/2$. (3) A non-vanishing transverse magnetic field during the sequences can be accounted for by a constant offset of B_-. When varying Δ during the sequence, these misalignments could tilt the spins and introduce spurious (background) excitations. (4) A misalignment of the probe field can be accounted for by extracting the signal $S = \mathrm{Re}[(1 + \mathrm{i}\epsilon_\parallel) S_-] + \epsilon_\perp N_a p_a / 2$ for $\epsilon_{\parallel,\perp} \ll 1$ (rather than simply $S = S_-$) from the simulation results.

We calculate the spectral map presented in Fig. 4b by repeating the calculation for $10.9\ \mathrm{mG} < B < 11.8\ \mathrm{mG}$ (corresponding to $-5 < \Delta/J < 5$ for $J = 47$ Hz, as used for normalizing Fig. 4). The excitation is simulated by applying $B_\perp(t) = 2.4\ \mathrm{mG} \times \exp[-t^2/(2.8\ \mu\mathrm{s})^2]$ ($\theta_a = 3°$). We calculate the Fourier transform of $\langle \hat{a} \rangle$ and the normalized amplitude $|\overline{\langle \hat{a}(\omega) \rangle}|$, as done for the experimental data. In Fig. 4b, we consider a perfectly aligned setup ($\beta_{x,y} = \eta_{x,y} = \epsilon_\parallel = \epsilon_\perp = 0$). In Fig. 4c, we reproduce the imperfection generating the perpendicular frequency branch by introducing a minute misalignment $\beta_x = 3.1$ mrad and $\beta_y = -\beta_x$. The calculations for Fig. 2a (solid lines) are done with $B = 11.33$ mG ($\Delta = -1.15J$) and $B_-(t) = 5.2\ \mathrm{mG} \times \exp[-t^2/(2.8\ \mu\mathrm{s})^2]$ ($\theta_a = 6.5°$).

Data availability

All data needed to evaluate the conclusions in the paper are present in the paper. The data that support the findings of this study and additional data are available from the corresponding author upon request.

References

38. Walker, T. G. & Happer, W. Spin-exchange optical pumping of noble-gas nuclei. *Reviews of Modern Physics* **69**, 629–642 (1997).
39. Vasilakis, G., Shah, V. & Romalis, M. V. Stroboscopic Backaction Evasion in a Dense Alkali-Metal Vapor. *Physical Review Letters* **106**, 143601 (2011).
40. W. Happer, Y.-Y. Jau, and T.Walker, Optically Pumped Atoms ISBN 978-3-527-40707-1 (WILEY-VCH, 2010)
41. Happer, W. & Tam, A. C. Effect of rapid spin exchange on the magnetic-resonance spectrum of alkali vapors. *Physical Review A* **16**, 1877–1891 (1977).
42. Romalis, M. V., Sheng, D., Saam, B. & Walker, T. G. Comment on "New Limit on Lorentz-Invariance- and C P T -Violating Neutron Spin Interactions Using a Free-Spin-Precession 3He -129Xe Comagnetometer". *Physical Review Letters* **113**, 188901 (2014).
43. Katz, O., Peleg, O. & Firstenberg, O. Coherent Coupling of Alkali Atoms by Random Collisions. *Physical Review Letters* **115**, 113003 (2015).
44. Duan, L.-M., Cirac, J. I., Zoller, P. & Polzik, E. S. Quantum Communication between Atomic Ensembles Using Coherent Light. *Physical Review Letters* **85**, 5643–5646 (2000).

Acknowledgements

We thank C. Avinadav and R. Finkelstein for fruitful discussions. We acknowledge financial support by the Israel Science Foundation, the European Research Council starting investigator grant Q-PHOTONICS 678674, the Minerva Foundation with funding from the Federal German Ministry for Education and Research and the Laboratory in Memory of Leon and Blacky Broder.

Author contributions

R.S., O.K. and O.F. all contributed to the experimental design, construction, data collection and analysis of this experiment. R.S. claims responsibility for all figures. The authors wrote the manuscript together.

Competing interests

The authors declare no competing interests.

Additional information

Extended data is available for this paper at https://doi.org/10.1038/s41567-022-01535-w.

Supplementary information The online version contains supplementary material available at https://doi.org/10.1038/s41567-022-01535-w.

Correspondence and requests for materials should be addressed to R. Shaham.

Peer review information *Nature Physics* thanks the anonymous reviewers for their contribution to the peer review of this work.

Reprints and permissions information is available at www.nature.com/reprints.

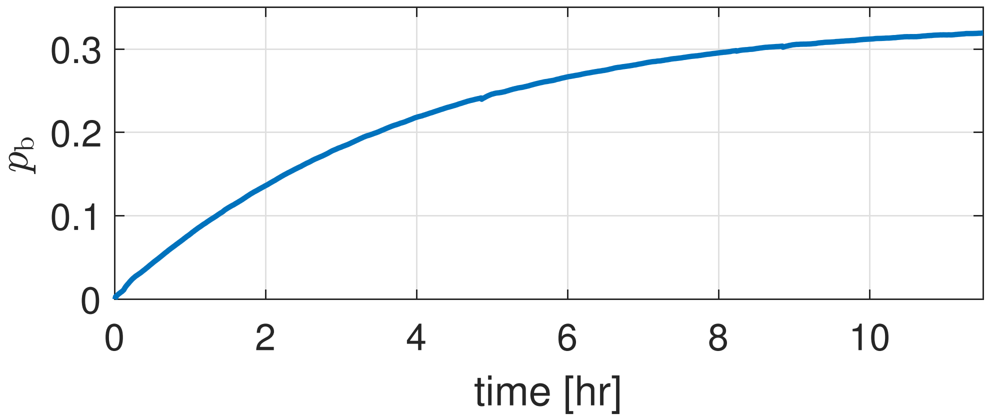

Extended Data Fig. 1 | Spin-exchange optical pumping. Typical measurement of the pumping process of helium-3 by optically pumped potassium vapor. Here the potassium density is $n_a = 4.9 \cdot 10^{14}$ cm^{-3}, and the helium depolarization time is $T_{1,\mathrm{act}}^{\mathrm{b}} = 3.9$ h.

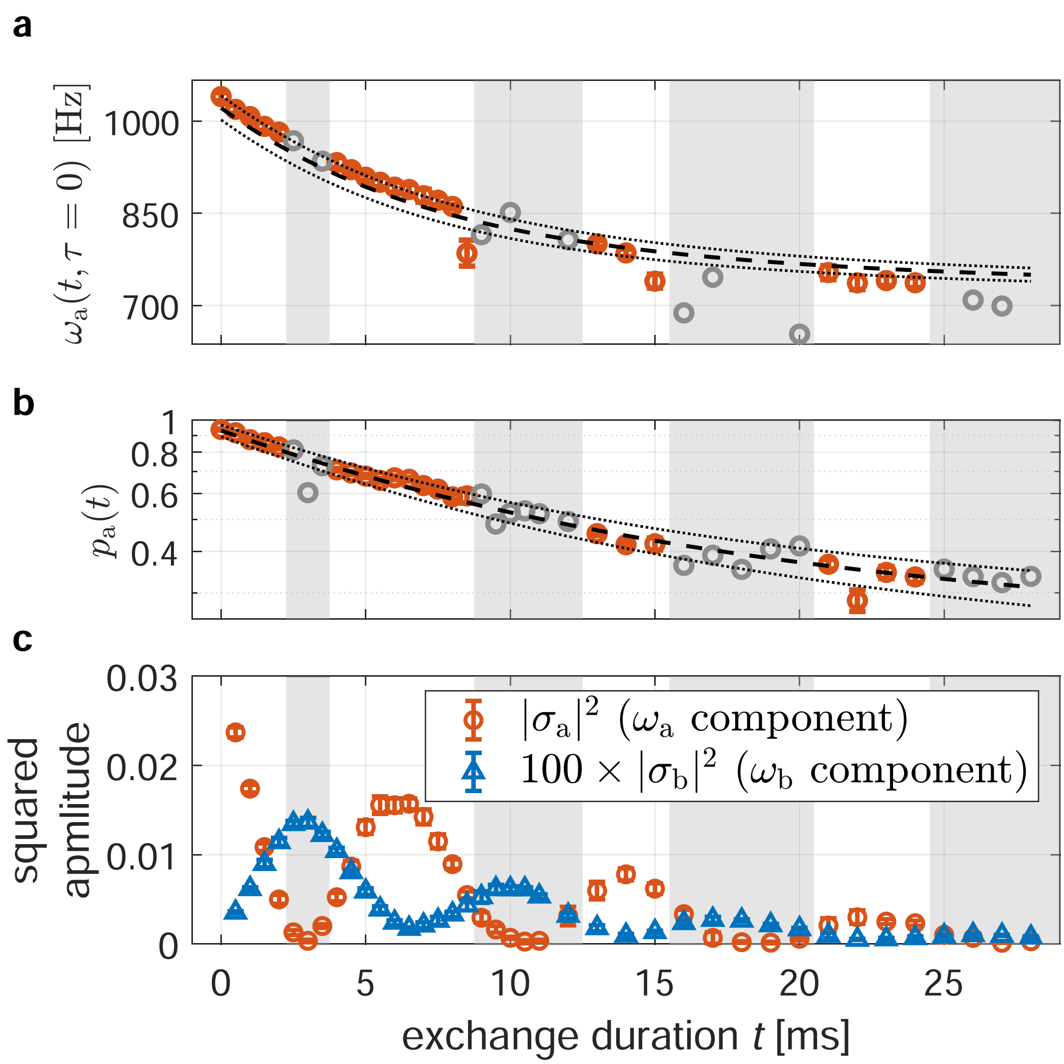

Extended Data Fig. 2 | Variables extracted from fitting Eq. (3) to the measured signals for each exchange time t, as exemplified in Extended Data Fig. 3. a. The change in alkali precession frequency $\omega_a(t, \tau = 0)$ [see Eq. (2)] manifests the change in the slowing-down factor due to alkali depolarization. **b**. The degree of alkali polarization $p_a(t)$ (in semi-log scale). In **a** and **b**, dashed black line correspond to the fitted multi-exponential model, and dotted lines present its confidence bounds. These are used as uncertainty estimations when using $p_a(t)$ to scale $\langle \hat{a} \rangle$ and $\langle \hat{b} \rangle$. Less reliable data, extracted when the excitations reside predominantly in the noblegas spins, are marked in gray. **c**. The two frequency components (amplitude squared) of the normalized Faraday rotation signal $\bar{S}_x(t + \tau)$. Note the factor of $(\Delta/J)^2 \gtrsim 100$ between them. Each data-point is averaged over 12 to 20 repetitions of the sequence.

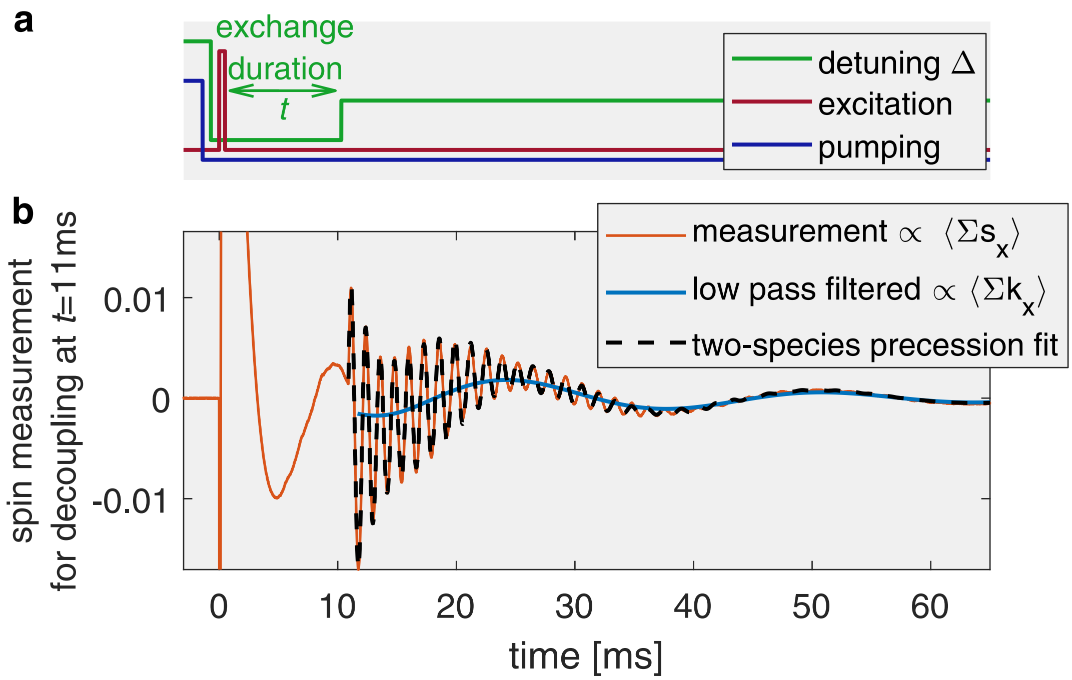

Extended Data Fig. 3 | Pulse sequence and typical results of an excitation-exchange measurement. a. First, we turn off the pumping and bring the two species to strong coupling with a small detuning Δ. We then generate a transverse excitation with a transverse magnetic field pulse. At a later time t, we halt the exchange by increasing the axial magnetic field and setting a large Δ. **b**. Example of a measured signal with exchange duration $t=11$ ms, with $\Delta=-1.15J$ before t, and $\Delta=790$ Hz $\gg J$ after t. We measure the alkali electron spin (red) which, once Δ is increased, can be used as a magnetometer that senses the noble-gas spin. The fast oscillations of the signal correspond to the Larmor precession of the alkali spin, and the slow modulation corresponds to the noble-gas precession. The latter is highlighted by the blue line (generated by low-pass filtering of the signal for illustrative purposes). We fit the signal to the model from Eq. (3) (dashed black line) and find the amplitudes of the alkali and noble-gas components at time t, which are used to estimate $\langle\hat{a}(t)\rangle$ and $\langle\hat{b}(t)\rangle$, respectively. The same fit also provides $p_a(t)$.